ACS OMEGA

Open Access

http://pubs.acs.org/journal/acsodf

Article

Synergistic Effect of Laser, Water Vapor, and Electron-Beam on the Degradation of Quasi-Two-Dimensional Ruddlesden–Popper Perovskite Flakes

Zhenfei Jiang,[#] Brian Ko,[#] Keith R. Berry, Jr., Xinxin Xing, Zhenhuan Yi, Alexei V. Sokolov, Jonathan Hu, Jiming Bao, and Zhenrong Zhang*

Cite This: *ACS Omega* 2024, 9, 35744–35756

Read Online

ACCESS | Metrics & More | Article Recommendations | Supporting Information

ABSTRACT: Understanding the effects of laser light, water vapor, and energetic electron irradiation on the intrinsic properties of perovskites is important in the development of perovskite-based solar cells. Various phase transition and degradation processes have been reported when these agents interact with perovskites separately. However, detailed studies of their synergistic effects are still missing. In this work, the synergistic effect of three factors (exposure to laser light, water vapor, and e-beam) on the optical and physical properties of two-dimensional (2D) Ruddlesden–Popper (RP) perovskite flakes [$(BA)_2(MA)_2Pb_3Br_{10}$] has been investigated in an environmental cell. When the perovskite flakes were subjected to moderate laser irradiation in a humid environment after prior e-beam irradiation, the photoluminescence (PL) peak centered at 480 nm vanished, while a new PL peak centered at 525 nm emerged, grew, and then quenched. This indicates the degradation process of the 2D RP perovskite was a phase transition to a three-dimensional (3D) perovskite [$MAPbBr_3$] followed by the degradation of 3D perovskite. The spatial distribution of the 525 nm PL signal shows that this phase-transition process spreads across the flake to the area as far as ~40 μm from the laser spot. Without humidity, the phase transition happened in the laser-irritated area but did not spread, which suggests that moisture enhanced the ion migration from the laser-scanned area to the rest of the flake and accelerated the phase transition in the nearby area. Experiments with no prior e-beam irradiation show that e-beam irradiation is the key to activating the 2D-3D phase transition. Therefore, when the three factors work synergistically, a conversion from the 2D RP perovskite into the 3D perovskite is not localized and propagates through the perovskite. These findings contribute to our understanding of the complex interactions between external stimuli and perovskite materials, thereby advancing the development of efficient and stable perovskite-based solar cells.

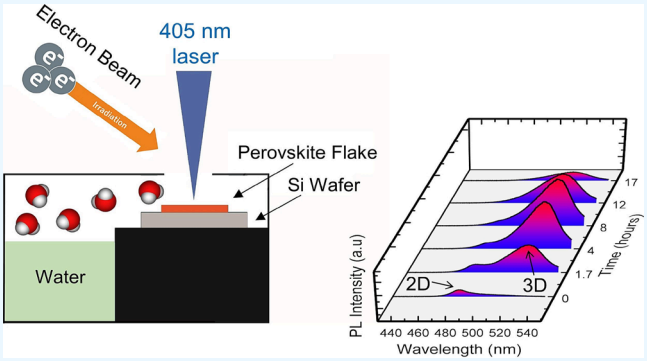

1. INTRODUCTION

Perovskites receive unprecedented attention due to their superior photoelectric properties, such as low exciton binding energy, low trap density, and high charge carrier mobility.[1−3] As early as 2009, by substituting dye organic molecules with organic−inorganic halide perovskite molecules such as methylammonium lead triiodide $CH_3NH_3PbI_3$ [MAPI], Kojima and collaborators explored the photovoltaic effect in a photoelectrochemical dye-sensitized cell and recorded that $CH_3NH_3PbI_3$ had power conversion efficiencies of 3.8%.[4] Although perovskites show good photovoltaic properties, the above low efficiencies were attributed to the dissolution of the perovskite material by the liquid electrolyte.[5] Attempts have been made to stabilize the perovskite material.[6−13] Compared to the traditional 3D organic−inorganic halide perovskites, 2D RP perovskites have received a lot of attention in photovoltaics because of their significant improvement in stability under exposure to light and humidity without sacrificing too much efficiency.[14−18] A right solvent design applied a 2D top layer of desired composition and thickness without destroying the 3D bottom layer (or vice versa). Such a cell would turn more sunlight into electricity than either 2D layers or 3D layers on its own with better stability. A recent development reports that the stability of 2D perovskites can be further improved by substituting butylammonium with (butylamino)-methaniminium cation.[19]

Understanding the degradation process of 2D RP layered perovskites facilitated by moisture, light, e-beam, and electric

Received: May 1, 2024
Revised: July 2, 2024
Accepted: July 30, 2024
Published: August 7, 2024

voltage is critical for the development of perovskite devices. Humidity is the primary cause of perovskite instability, which ultimately affects the surface morphology and device performance.[20−24] The interaction between moisture and 2D, 3D, or mixed perovskites has been investigated by many groups. For the MA-based 3D perovskite, the initial monohydrate phase is reversible and followed by complete decomposition to PbI_2 and H_2O.[25,26] For the more stable 2D RP perovskite,[14,27] two mechanisms of moisture-induced degradation were reported. A larger-*n* *n*-butylammonium methylammonium lead iodide (*n*BA-MAPI) phase could degrade into a more stable, protective, low-n surface layer and a 3D MAPI phase,[24,27,28] or it could directly degrade into a stable $n = 1$ phase.[29]

The laser irradiation introduces photothermal heating and photo-oxidation.[30−32] For the 3D perovskite, before complete degradation, the enhancement of PL intensity upon light irradiation has been reported and was attributed to the redistribution of the halide ions[30] and photo-oxidation[32] as a part of the light soaking effect. The laser-induced PL quenching effect due to the decomposition of 2D perovskites has also been reported previously.[33,34]

Although there is no e-beam exposure during the operation of perovskite solar cells, perovskite is under the influence of electric bias-induced charge diffusion. In addition, scanning electron microscopy (SEM) and transmission electron microscopy are typical techniques used to investigate changes in the structure, surface morphology, and elemental compositions of materials after solar cell testing. During the e-beam scanning process, the unintentional doping due to charge accumulation, the elastic scattering, and the electric field introduced from the irradiation of the energetic electrons can alter the physical and the chemical properties of perovskites.[35−38] Even moderate e-beam irradiation (10 kV, ∼1 nA) could drive degradation of the 3D MAPI perovskite[35,37,38] and induce the quenching of the PL and CL signal.[35,37] Therefore, understanding the impact of the e-beam on the properties of perovskite during characterization is critical. Different degradation mechanisms have been reported including defect (halide vacancies and interstitials) formation caused by irradiation damage,[35,37,38] phase transition induced by e-beam heating,[35] and e-beam introduced ion migration.[37] The e-beam-induced degradation is reported to be permanent and irreversible. The formation of the defect would cause quenching of the PL due to trapping of the excitons and their nonradiative recombination. As for the 2D perovskite, it is not clear whether the effect of the e-beam on its degradation is similar to that of the 3D perovskite.

The stability of the perovskite in solar cell operations is impacted by the synergy of several stimuli, including light illumination, oxygen and water vapor exposure, heat, and applied electric field. The impact of some of the individual factors (e.g., laser, water vapor, and energetic electron beam) on the stability of perovskites has been studied. However, their synergistic effects on the degradation of 2D RP perovskites are scarce. In this work, we conducted time-dependent PL mapping under various conditions (with/without prior SEM scanning and with/without added humidity) to identify the isolated and combined roles of these three factors on the optical characteristics of 2D RP perovskite flakes. The change of the PL intensity at the laser-scanned area shows that there were two different decomposition processes determined by prior e-beam scanning. Even moderate e-beam irradiation triggered a 2D/3D phase transition whether there was added humidity or not. The 2D RP perovskite flake underwent direct decomposition when prior SEM imaging was not conducted. In addition, the effect of the laser-scanned area on the optical properties of the rest of the entire flakes has been studied. Added humidity promoted the propagation of the decomposition from the laser-scanned area to the rest of the flake. The observed inhomogeneity in PL on the flakes was a result of a delicate balance among these synergistic factors (laser exposure, water vapor, and electron-beam irradiation) in the degradation processes of 2D RP perovskites. This work paves the way for advancement of the stability of perovskites in solar cell applications.

2. EXPERIMENTS

2.1. Synthesis of $(BA)_2(MA)_2Pb_3Br_{10}$. The synthesis of butylammonium methylammonium lead bromide, $(BA)_2(MA)_2Pb_3Br_{10}$, has been reported previously.[39] Briefly, crystals were synthesized by dissolving the precursors PbO (0.59 mmol, 131.7 mg, Sigma-Aldrich), BABr (0.19 mmol, 29.3 mg, Sigma-Aldrich), and MABr (0.4 mmol, 44.8 mg, Greatcell Solar) in an acid mixture consisting of 0.9 mL of HBr (Sigma-Aldrich) and 0.1 mL of H_3PO_2 (Sigma-Aldrich) in a 10 mL glass vial. Using a magnetic stir rod, the vial was heated to 393 K in an oil bath.[39] After the precursors were completely dissolved and the solution became transparent, the stirring was stopped, and the solution was cooled at a rate of 2 K/min during which crystals were formed. The crystals were collected via filtration, and the residual solvent was removed by a vacuum pump. The UV−vis absorption spectra confirmed that *n* is 3. The perovskite flakes were prepared via mechanical exfoliation and deposited onto a piece of Si wafer to allow for reflection-based PL measurements, while also preventing charging effects from occurring during the SEM measurement. The Si wafer was cut using a diamond scribe and cleaned via sonication first in acetone and then in 96% ethanol solution.

2.2. Experimental Setup. The laser effect was tested via a time series PL mapping measurement using a lab-built PL microscope. Water vapor was regulated via an environmental cell (Figure 1). E-beam irradiation was performed via scanning electron microscopy (SEM, FEI Co., Versa 3D). The sequence of various optical and physical properties measurements of the flakes is shown in Figure S1. After sample preparation, a Leica camera was used to take optical images of the 2D RP

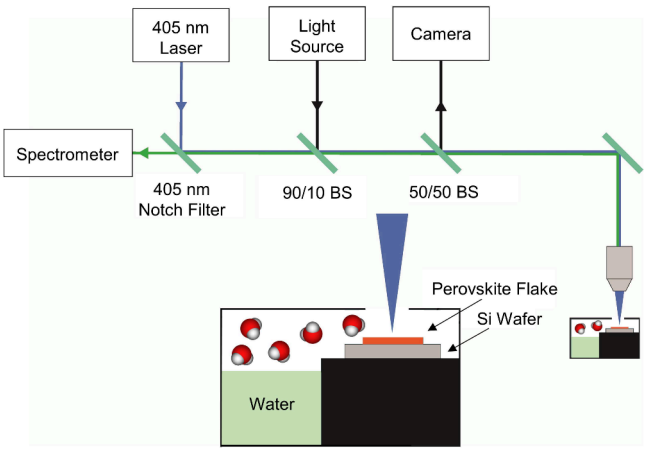

Figure 1. Setup for the time series PL mapping of the 2D RP perovskite flakes in an environmental cell.

https://doi.org/10.1021/acsomega.4c04188
ACS Omega 2024, 9, 35744−35756

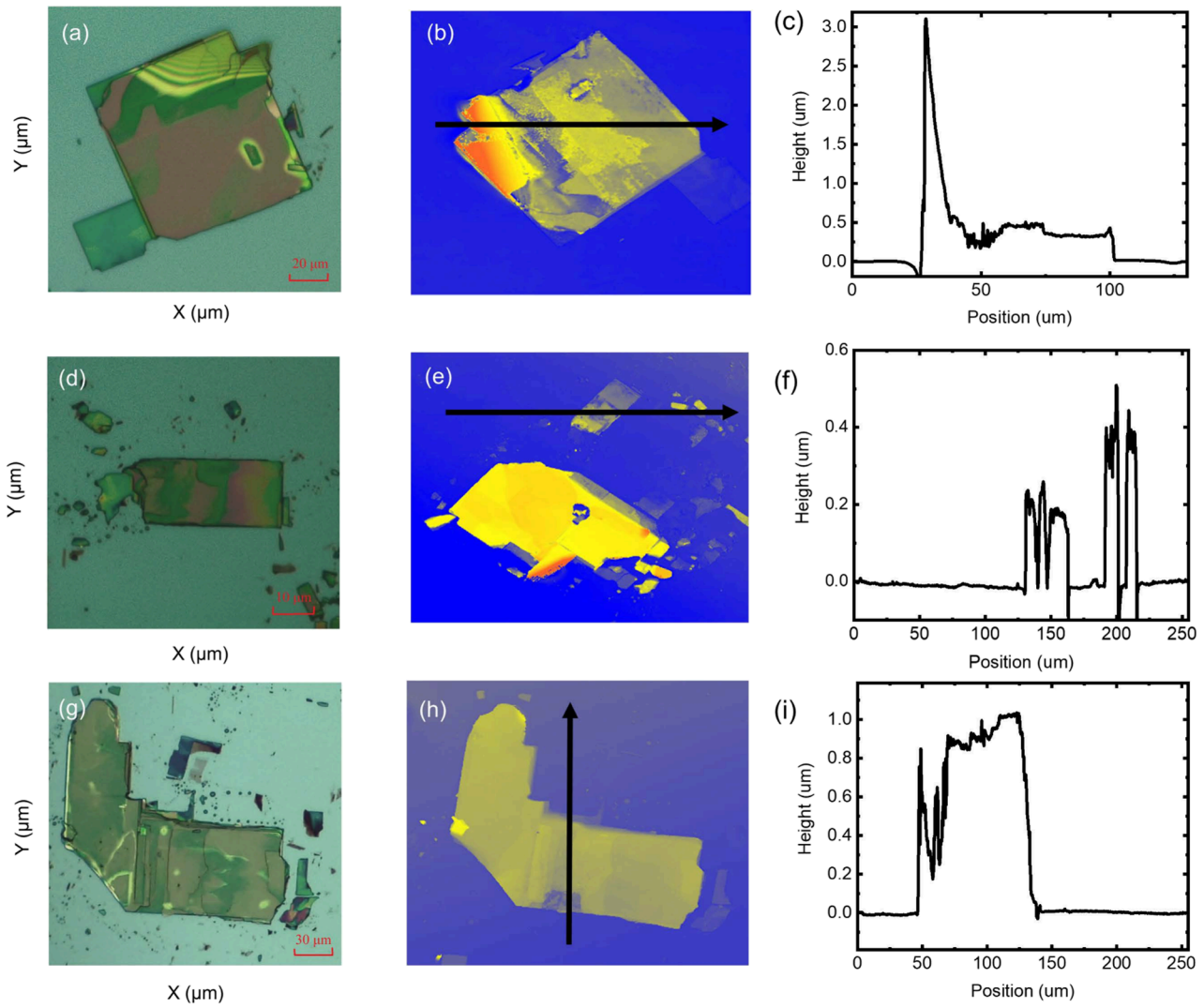

Figure 2. Overview of 2D RP perovskite flakes and their height information. (a, d, g) Optical images of the 2D RP perovskite flakes before time series laser scanning; (b, e, h) corresponding height maps that were measured by 3D-LSM after the time series laser scanning experiments; (c, f, i) corresponding height profiles along the arrows depicted in panels (b), (e), and (h). Typical height is between 0.2 and 1 μm, except an area reaches 3 μm in panel (c). In the time series experiments, the flakes in panel (a) were exposed in the humid environment during the time series laser scanning with prior e-beam irradiation; the flakes in panel (d) were in the dry environment during the time series laser scanning with prior e-beam irradiation; the flakes in panel (g) were exposed in the humid environment during the time series laser scanning but without prior e-beam irradiation.

perovskite flakes. Confocal laser scanning microscopy (CLSM, Olympus, FV-3000) measurements (405 nm surface-scanning excitation, 440−700 nm collection) were performed to provide a PL map and reference PL spectra. Then, the sample was scanned using SEM (if done) to measure the morphology of the perovskite flakes before continuous laser exposure. The SEM scanning was operated at 15 kV with a current of ∼0.1 nA. Afterward, the sample was put in the dry environmental cell. The SEM maps were used as a map to locate the flake, and a PL map was taken via the lab-built PL spectroscope (Figure 1). Briefly, a CW laser (405 nm, 4 mW, Thor Laboratories L405P20 laser diode) was focused onto the sample, and the back-reflection is then diverted to a spectrometer (Princeton Instruments IsoPlane-320) using a notch filter to remove the excitation laser. After the initial map, a time series of PL maps is taken consecutively on a small fraction of the area using the lab-built PL microscope, with an optical image taken in between the maps.

As shown in Figure 1, the sample was placed in an environmental cell for the time series PL mapping experiment. The Si substrate holding the perovskite flakes was placed on a platform in the cell. For experiments that required an environment with increased humidity, a pool of distilled water was added next to the platform. The relative humidity in the cell was ∼87%. The lid of the cell had a hole that allowed only water vapor and air to escape by passing by the flakes. The series continued for about 15 h, usually overnight. After the time series was completed, a final PL map of the entire perovskite flake was measured. For the experiments with no water vapor, the samples were placed in a dry environmental cell.

After continuous PL mapping, SEM and CLSM measurements were taken with identical conditions to the pretime series measurements for comparison. Afterward, the 3D-laser scanning microscopy (LSM, Olympus OLS5100 LEXT) was used to determine the thickness of the flake at the time series

https://doi.org/10.1021/acsomega.4c04188
ACS Omega 2024, 9, 35744−35756

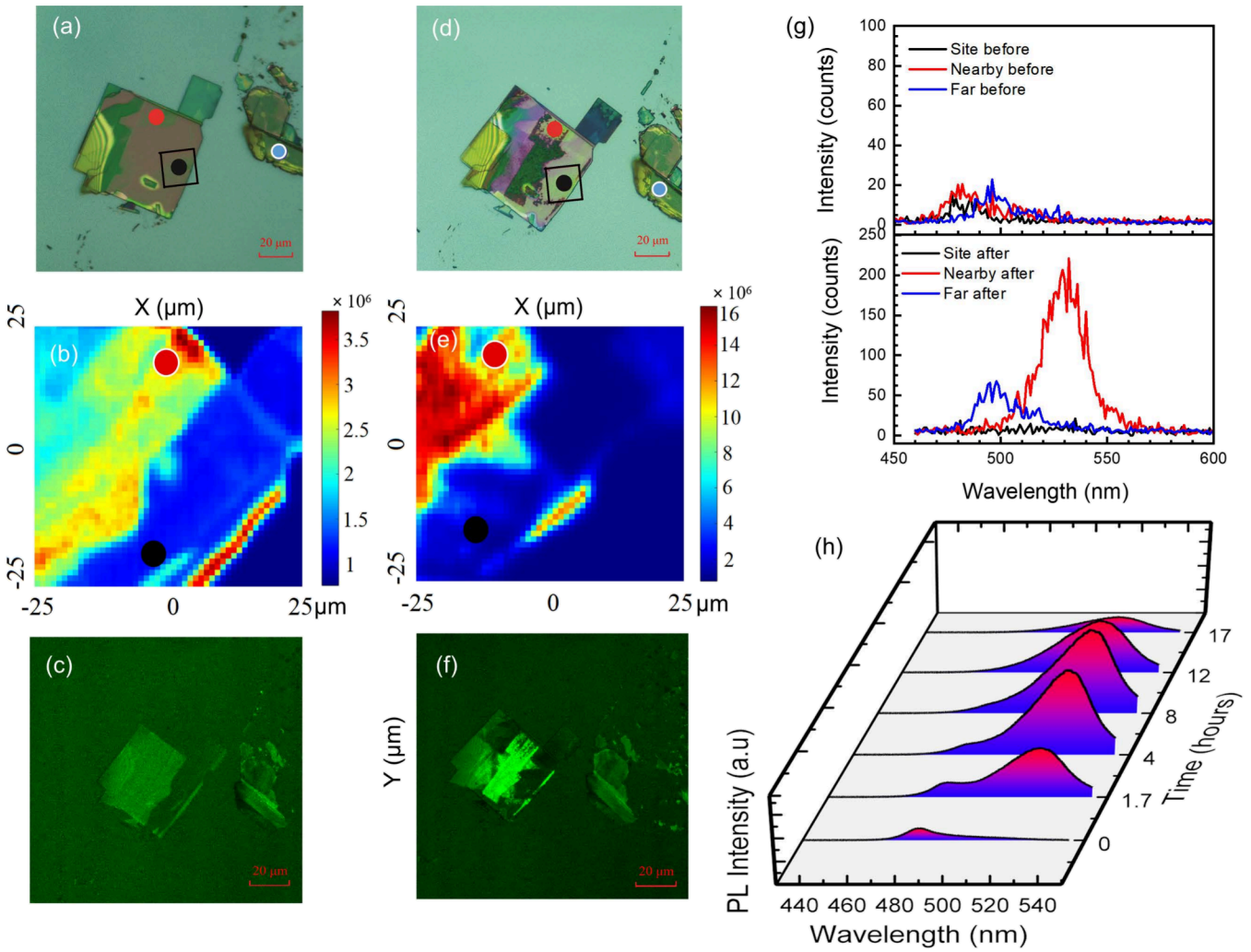

Figure 3. Optical properties of the 2D RP perovskite flakes before, after, and during a PL mapping time series in a humid environment after SEM scanning. (a, d) Optical images of the 2D flakes taken before and after laser irradiation in time series. The black box together with a black dot denotes the laser-scanned area during the time series. The red dot denotes the nearby area within the same flake. The blue dot denotes the far area in a different flake. (b, e) Corresponding PL maps taken before and after the time series measurements using PL microscopy. (c, f) PL maps taken before and after the time series measurements using CLSM. (g) The PL spectra averaged from extended areas marked by the red, black, and blue dots in panel (a) taken before (top) and after (bottom) the time series via CLSM. (h) The time-dependent PL spectra at laser scan area during the time series measurements using PL microscopy.

exposure site and the surroundings (Figure 2). The 3D-LSM measurements showed that the 2D RP perovskite flakes vary in thickness from approximately 0.5 to 3 μm, well pass the mono- or few-layer thickness regime. We chose thicker flakes because, in general, the perovskite layer in solar cells is about to a few hundred of nanometers thick and because the diffusion length plays a key role in the photovoltaic performance of perovskite solar cells.[14−17]

3. EXPERIMENTAL RESULTS

3.1. Characterization of Flakes under the Exposure of Laser, Water Vapor, and Prior E-Beam Irradiation. The synergistic influence of three factors (laser illumination, water vapor, and e-beam irradiation) on the 2D RP perovskite flakes was investigated by monitoring the optical and physical characteristics of the flakes before, during, and after the PL time series experiment. The optical images (Figure 3a,d) and SEM images (Figure S2) taken before and after the time series experiment show the morphology of the selected perovskite flake and regions of interest. The surface of the flake was smooth and flat (Figure S2a). The thickness of the flake was about 0.5 μm (Figure 2c). During the PL time series measurement, the entire sample was in a humid environment, and only a fraction of the flake marked by the black box in Figure 3a was directly subjected to a 405 nm laser irradiation. The red dot denotes the nearby area within the same flake, and the blue dot denotes the far area in a different flake.

Two PL maps each were collected to provide optical characteristics of flakes before and after the time series measurement, one using CLSM (Figure 3c,f) with a large field of view and the other (Figure 3b,e) taken in the environmental cell using PL microscopy with a high signal-to-noise ratio and a high spectral resolution. Both PL maps (Figure 3b,c) taken before the time series show the inhomogeneity of the PL intensity, for example, the integrated PL intensity (from 450 to 700 nm) at the black dot marked area is weaker than that of red dot marked area. The PL spectra from various locations on the flake show a 480 nm peak, which corresponds to the band gap of the 2D hybrid perovskite[39] as shown in Figures 3g and

https://doi.org/10.1021/acsomega.4c04188
ACS Omega 2024, 9, 35744−35756

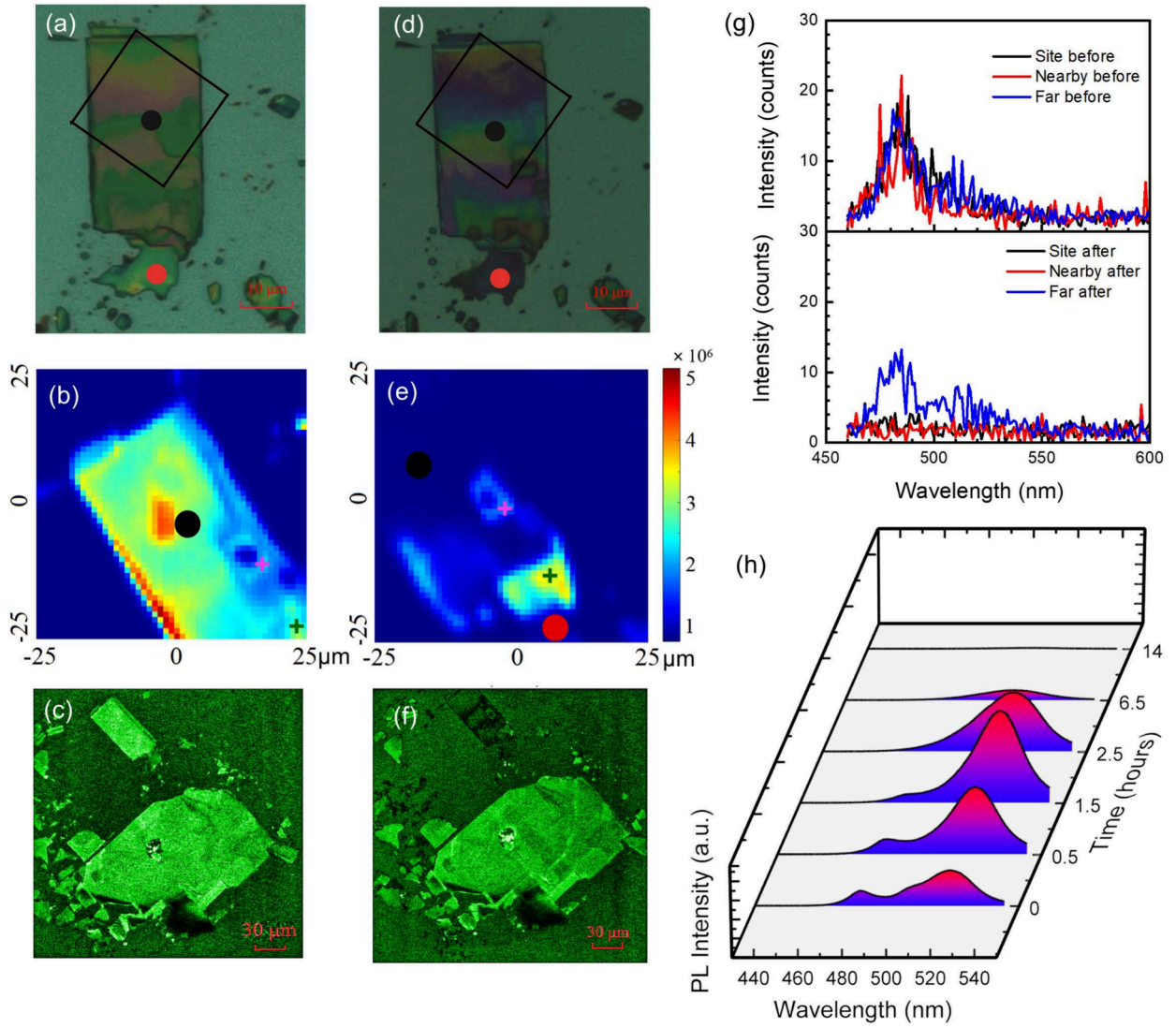

Figure 4. Optical properties of the 2D RP perovskite flakes before, after, and during a PL mapping time series in a dry environmental cell after SEM scanning. (a, d) Optical images of the 2D flakes before and after laser irradiation in time series. The black box with a black dot denotes the laser-scanned area during the time series, and the red dot denotes the nearby area within the same flake. (b, e) Corresponding PL maps taken before and after the time series measurements using PL microscopy. The pink cross and the green cross marked the high-flux e-beam irradiated areas. (c, f) PL maps that were taken before and after the time series measurements using CLSM. (g) The average PL spectra taken before (top) and after (bottom) the time series via CLSM at the red dot and the black dot marked areas in panel (a) and a separate flake. (h) The time-dependent PL spectra at laser scan area during the time series using PL microscopy.

S3. The spectra also show a small peak around 510 nm in some areas, which is an indication of a small amount of 3D perovskite often appeared at the edge of $MAPbBr_3$ nanocrystals.[40]

A series of PL maps were then taken consecutively for 17 h on the area marked by the black box in Figure 3a with added humidity, with an optical image taken between PL maps. After the time series was completed, the optical properties of the 2D RP perovskite flake changed significantly. The integrated PL intensity (black spectrum in Figure 3g) of the laser-scanned area (marked by the black dot) was quenched. Note that the intensity scale range in Figure 3e is larger than that in Figure 3b. Different nearby areas on the flake showed different spectral signatures (Figure S3). In an extended nearby area (marked by the red dot), the integrated PL intensity increased significantly (Figure 3e,g lower panel). This area is on the same flake as the black dot marked area, but it is not directly exposed to the laser. The average spectrum over this extended bright area (red spectrum in the lower panel of Figure 3g) shows that the 480 nm peak is completely quenched, and a new PL peak at about 525 nm appeared. The peak intensity of the 525 nm PL peak is 10 times higher than the 480 nm PL peak intensity before the time series. The 525 nm PL peak has been identified to correlate with 3D perovskite and the 2D/3D perovskite heterostructure that is often observed as the edge emission.[39,41−44] Wang et al. discovered that the edge has a much higher electrical conductivity than the center region.[45] The appearance of the 525 nm PL peak is an indication that the 2D perovskite experienced a 2D to 3D phase transition during continuous laser scanning. Other nearby areas experienced the quenching in the 2D PL intensity and emerging of a low intensity of the 3D peak at 525 nm (purple dot and green dot marked areas in Figure S3). SEM images (Figure S2b,c) taken after the time series show the morphological change of the

https://doi.org/10.1021/acsomega.4c04188
ACS Omega 2024, 9, 35744−35756

flake. The area under direct laser excitation, marked by the black dot, was smooth. The nearby area, marked by a red dot, was no longer smooth and was covered by patches of grains. The corresponding 525 nm PL peak (Figure S3) suggests that these grains are the 3D perovskite grains.[25,39] The variation in the thickness and roughness of the whole flake can be seen in the color change of the flake in the optical image (Figure 3d).[46]

The time-dependent PL spectra at the laser-scanned site marked by the black box with a black dot in Figure 3a have been further investigated. Representative spectra are displayed in Figure 3h. As laser irradiation time increased, the intensity of the peak centered at 480 nm stayed almost constant for the first several hours, followed by a slow decrease, and disappeared eventually. This means that the 2D RP perovskite was decomposed after prolonged laser irradiation in a humid environment. The peak centered at about 510 nm was inconspicuous at the beginning, then emerged, and kept on growing to reach an intensity that is about 8 times the 480 nm PL peak intensity before the time series. While growing, this peak continuously redshifted to 525 nm, which indicates the 2D to 3D phase transition. After the flake was under laser irradiation for a prolonged time (8 h) in water vapor, the 525 nm peak began to decrease and eventually reduced to an intensity that was comparable to that of the 480 nm PL peak before the time series.

The progress of the PL at the laser-scanned site suggests that after the PL time series, the nearby area marked by the red dot showed a PL spectrum (red spectrum in Figure 3g bottom) that mimics a spectrum that was in the process of the transformation from 2D to 3D perovskite. The low PL intensity (Figures 3g and S3) from additional nearby areas indicates that they were in various stages of degradation. Therefore, the PL of the whole flake was affected even though the laser irradiation was conducted in one confined area.

The prior SEM scanning may have some impact on the inhomogeneity of the PL. For example, the straight lines on the SEM images can be traced back to the prior low-flux e-beam scanning. However, it is not the direct cause of the difference between the high PL area and the low PL areas. For example, the red cross and the black cross marked areas in Figure S2 experienced the same e-beam scanning showing very different PL intensities in Figure 3f.

Additionally, a reference spectrum (the blue spectrum in Figure 3g) taken on a separate perovskite flake that was not subjected to laser exposure but under the influence of humidity shows that the PL intensity of this flake had an observable increase after the time series, while the PL peak position remained the same. This is different from the change of PL at the nearby area marked by the red dot where a new peak emerged at 525 nm with high PL intensity. For the 3D perovskite, the enhancement of the PL intensity in moisture was reported previously and was attributed to the passivation of the various bulk and surface defects.

To separate the synergistic effect of laser exposure, increased humidity, and e-beam irradiation, two sets of control experiments were conducted: one with no water (see section 3.2), and the other without prior e-beam irradiation (see section 3.3).

3.2. Characterization of Flakes under the Exposure of Laser and E-Beam with No Moisture. In this section, a similar set of experiments was conducted but in a dry environment cell. Figure 4 shows the optical characteristics of a 2D RP perovskite flake taken before, during, and after the time series. Different from the results in the humid environment (section 3.1), the PL intensity of the whole flake and a separate flake (far area) did not increase after the time series. The PL is quenched on the entire flake (Figure 4e,f) except for two bright spots (marked by pink and green crosses) that experienced high-flux (~100k e $Å^{-2}$ s^{-1} at 15 kV) e-beam irradiation before the time series (Figures 4e and S5). The intensity of the 480 nm PL peak at both the laser-scanned area (black spectrum) and its nearby area (red spectrum) decreased to baseline (Figure 4g). However, the main difference is that there was no growth of the peak at 525 nm at nearby areas (Figure S5) in comparison to the spectra obtained with water vapor.

The time dependence of PL at the laser scan site (black box in Figure 4a) has been further investigated. As shown in Figure 4h, at the start of the time series, this area showed two main PL peaks at 480 and 525 nm indicating that it contained both 2D RP perovskite and 3D perovskite. Note that the CLSM spectra (Figure 4g) were collected before the flake was exposed to the e-beam and showed no 525 nm peak. The appearance of the 525 nm peak indicates that after SEM imaging, a phase transition from 2D to 3D in the e-beam irradiated area was activated. During the time series, the trends of the change of the PL at the laser irradiated area with (Figure 3h) and without water vapor (Figure 4h) were similar. Specifically, the peak centered at 480 nm did not change at the beginning and then gradually disappeared. The peak centered at 515 nm redshifted to 525 nm while its intensity grew considerably (~2.5 times) in the 90 min, which means the 2D to 3D perovskite transformation continued during the time series. This result shows that H_2O is not a necessary factor for the 2D-3D phase transition. After more than 90 min of prolonged laser exposure, the 525 nm peak also started to decline, and the 3D perovskite PL was completely quenched after 7 h.

Unlike the experiment with humidity, the 2D to 3D phase transition did not spread to the rest of the flake, even in the area with high-flux e-beam irradiation. Before the time series scanning, the low-intensity peak around 515 nm was observed in most of the areas on this flake in PL spectra (Figure S5) after the whole flake was irradiated with moderate e-beam flux (~100 e $Å^{-2}$ s^{-1} at 15 kV). This 3D peak was also observed in some areas on the flake before the time series in section 3.1. Relatively high-intensity ~515 nm peak appeared at the high-flux e-beam irradiated areas. After the time series, the 2D peak at 480 nm was quenched in all these nearby areas, but the 3D peak kept almost the same intensity unlike the large increase observed in the laser-scanned area.

In the far area (blue spectrum in Figure 4g), which was not exposed to the e-beam and with no laser exposure, the peak shape and intensity remained almost the same. Evidently, the increase in PL at the far area in the experiment with water vapor in section 3.1 should be attributed to added humidity.

SEM images (Figure S4) show that there are barely noticeable changes in the smoothness of the flake in both the laser-scanned area and the vicinity. Unlike the results obtained with water vapor, no grainy patches were formed on the entire flake, including the laser-scanned area. In addition, the few areas irradiated by high-flux (~100k e $Å^{-2}$ s^{-1} at 15 kV) e-beam appear as bright rectangular areas with some damage. These areas experience large electron doping. Hence, the appearance of the high-intensity 525 nm PL peak at the

https://doi.org/10.1021/acsomega.4c04188
ACS Omega 2024, 9, 35744−35756

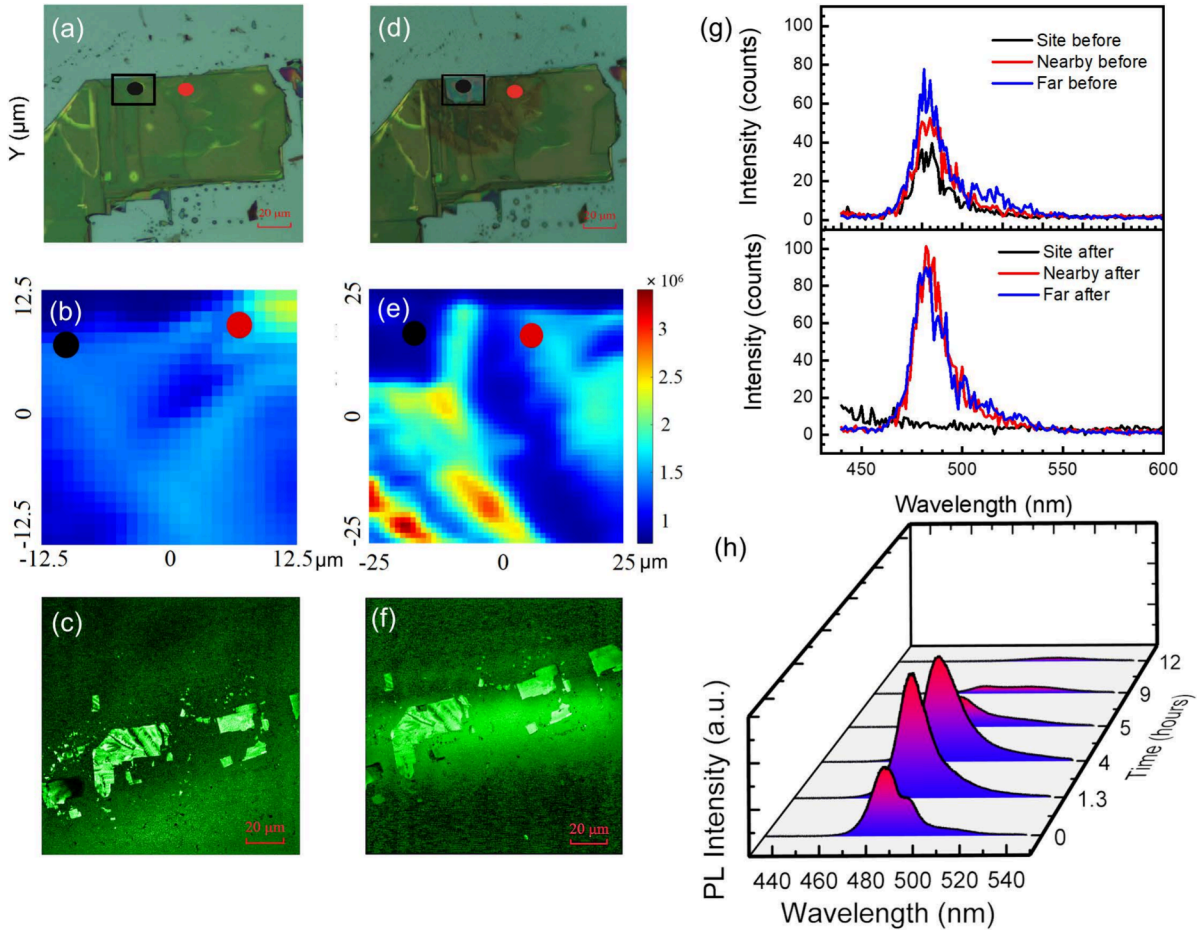

Figure 5. Optical properties of the 2D RP perovskite flakes before, after, and during a PL mapping time series in a humid environment without prior SEM scanning. (a, d) Optical images of the 2D flakes before and after continuous laser scanning in time series. The black box with a black dot denotes the laser-scanned area during the time series, and the red dot denotes the nearby area within the same flake. (b, e) Corresponding PL maps taken before and after the time series measurements using PL microscopy. (c, f) PL maps that were taken before and after the time series measurements using CLSM. (g) The averaged PL spectra taken before (top) and after (bottom) the time series via CLSM at the red dot and the black dot marked areas in panel (a) and a separate flake. (h) The time-dependent PL spectra at laser scan site during the time series using PL microscopy.

high-flux e-beam dosage area is consistent with the high electrical conductivity that was observed at the edge state.[45]

3.3. Characterization of Flakes under the Exposure of Laser and Water Vapor: No Prior E-Beam Irradiation. Different sets of control experiments were conducted on new flakes with added humidity in the environmental cell but without e-beam irradiation before the time series experiment. The main difference from the flakes experienced prior e-beam irradiation is that there was no 525 nm peak that appeared anywhere on the flake during and after the time series experiment.

Before the time series, the 480 nm 2D PL peak appeared consistently throughout the flake (Figure 5g) with no obvious peak from 510 to 525 nm, as no e-beam irradiation was performed. After the time series, the laser-irradiated region showed a quenched PL signal (Figure 5g), due to the degradation of the flake. The rest of the flake showed an increase in the intensity of the 480 nm PL peak (red spectrum in Figures 5g and S7). In the far area on a separate flake, which was only affected by the humidity, the PL intensity at 480 nm had a noticeable increase (blue spectrum in Figure 5g). The increase was clearly due to the added humidity, which is consistent with the change of PL intensity in the far area from the previous experiment in section 3.1.

The change of the PL at the laser scan site (black box in Figure 5a) has been further investigated (Figure 5h). At zero time, the 480 nm peak is accompanied by a shoulder at 495 nm. This 495 nm peak could be attributed to a small amount of quasi-RP perovskite with n = 5.5, which was observed during synthesis, which has been observed previously.[39] During laser irradiation, the intensity of the 480 nm peak almost doubled after about 1.3 h. Upon further laser irradiation, it began to diminish and eventually completely quenched, as expected. In comparison to the experiments with prior e-beam irradiation (sections 3.1 and 3.2), no peak at 525 nm emerged and grew during the laser irradiation. This implies that the flake did not contain a newly generated 3D perovskite phase. Therefore, it is reasonable to conclude that the generation of 3D perovskites can be attributed to the effect of e-beam irradiation. Laser irradiation did not create these nucleation sites. Exposure to H_2O vapor did not create the 3D nucleation sites either.

After the time series, the irradiated region (black dot) was degraded (Figure 5d), leaving a thin perovskite layer surrounded by a darkened region as shown in Figure 2h,i. SEM image (Figure S6) shows that the laser-scanned area is

https://doi.org/10.1021/acsomega.4c04188
ACS Omega 2024, 9, 35744−35756

smooth after the time series. The morphology of the surrounding area changed. Brighter veins formed and spread out from the laser-scanned area. High-magnification image shows that these veins are a mixture of grains and flake patches.

4. DISCUSSION

In this section, the separate roles and synergistic effects of laser, water vapor, and e-beams on the degradation of 2D perovskite will be discussed.

4.1. Role of Laser. In the laser scanning areas, laser irradiation played a dominant role in all three sets. The PL intensity of perovskite flakes had an initial increase and was eventually quenched at the laser-scanned area due to the flakes' degradation. This observation is consistent with the reported light-induced decomposition of perovskite.[2,17,33] The enhancement of PL intensity upon light irradiation has been reported for the 3D perovskite and was attributed to the redistribution of the halide ions[30,47] and photo-oxidation[32] as a part of the light soaking effect. The photogenerated electron would fill the electronic traps. The generated electric field induces the segregation of the halide ions and their migration from the laser-illuminated area to the surrounding area. The mobile halide ions fill the halide vacancies and yield a reduction in the density of shallow and deep traps, which are responsible for the nonradiative recombination, resulting in PL brightening in the illuminated area. Additionally, the increased temperature from laser irradiation increases the ionic conductivity. In the presence of oxygen, photo-oxidation-generated oxygen-related species and photogenerated carriers could passivate the vacancy and deactivate the trap sites.[32,48] The photo-oxidation-generated oxygen-related species undermine the chemical stability of metal halide perovskites while surprisingly improving their optical properties.[32] The theoretical calculations show that the material degradation and charge carrier lifetimes depend strongly on the oxidation state of the oxygen species.[49] The peroxide eliminates the trap states and improves the PL intensity. Other reports showed a continuous decrease PL intensity in air and in solution, which is attributed to the generation of superoxide and the subsequent oxidative disintegration of $MAPbI_3$.[50,51] The laser-induced PL quenching effect due to the decomposition of 2D perovskites has also been reported previously.[33,34] In these reports, the PL spectrum shape and position have a little change, and no new PL peak has been reported.

In this work, two different degradation processes were observed depending on whether the flakes experienced prior e-beam irradiation. With prior e-beam irradiation, the growth and the diminishment of the 525 nm PL peak suggest that laser irradiation sped up the processes of 2D RP perovskite to 3D phase transition and their degradation (sections 3.1 and 3.2). This phase transition process spreads to the nearby areas when moisture was present, as displayed in section 3.1 (see the discussion below). The structure of 3D perovskites collapsed eventually under prolonged laser exposure, causing PL quenching. Without prior e-beam irradiation, laser illumination accelerated the rates of hydration in a humid environment, showing enhanced PL intensity (section 3.3). 2D perovskite further directly decomposed without phase transition. The laser heating amplified the spreading of the direct decomposition from the laser-scanned area to the nearby areas.[2]

4.2. Role of Water Vapor. The separate role of humidity on the optical properties of 2D perovskites can be inferred from PL spectra in the far area in the three sets of experiments. The far areas were on separate flakes, which were free from continuous laser illumination and prior e-beam irradiation. The PL intensity centered at 480 nm has an observable increase and no new PL peak emerges when these areas were only exposed to water vapor during the time series in sections 3.1 and 3.3. On the contrary, no increase in intensity was observed in experiments conducted without water vapor (section 3.2). Therefore, the noticeable increase in the PL intensity at 480 nm was due to the presence of added humidity.

Humidity has been an important factor in the stability of the perovskites. The interaction between moisture and 2D, 3D, or mixed perovskites has been investigated by many groups. For the 3D perovskite, the enhancement of the PL intensity without change in peak position has been reported with post-treatment in humidity.[25,26,52] The enhancement was attributed to the passivation of the various bulk and surface defects. When water molecules diffuse and penetrate the perovskite, the dissolution of the perovskite component, most likely alkylammonium, and their recrystallization would passivate the trapping defects.[28,52] After prolonged exposure, the redshift of the PL together with enhanced PL intensity has been observed, which was attributed to the structural disorder introduced when H_2O molecules are incorporated in the lattice.[25,26] For the more stable 2D RP perovskite,[14,27] two mechanisms of moisture-induced degradation were reported. A larger-n nBA-MAPI phase could degrade into a more stable, protective, low-n surface layer and a 3D MAPI phase.[24,27,28] Another mechanism is the degradation of the larger-n phase directly into the stable n = 1 phase and MAI and PbI_2.[29] In both degradation processes, the blueshift of the peak position was observed, which is a signature of the low-n 2D phase accompanied by the reduced PL intensity.[24,28]

In our study, the 2D perovskite showed an enhanced PL intensity after prolonged (>12 h) humidity exposure, which confirms the improved stability of quasi-2D RP phase organolead halide perovskites. This is the first report on the enhancement of PL of the 2D RP perovskite when exposed to moisture. No blueshift of the PL peak under prolonged humidity exposure is observed in our results indicating that there was no low-n (n < 3) nBA-MAPBr formation in the far areas. The increase of the PL indicates the passivation of the defects, which reduced the number of the trap densities similar to the 3D perovskite.

As for the laser-scanned area, laser-induced heat accelerated the rate of hydration. The moisture-induced processes, the solubilization of the alkylammonium, and the recrystallization were amplified. In addition, the redistribution of the halide ions would be faster, and the rate of photo-oxidation would increase too due to laser heating. All these processes could reduce the density of trapping defects.[28,35,48,52] They contribute to the initial enhanced PL in the laser-scanned area in section 3.3 (Figure 5h). Interestingly, without e-beam irradiation, there was no 2D-3D phase transition, even in the laser-scanned area. This indicates that e-beam irradiation is a critical factor in activating the 2D-3D phase transition.

The nearby area in section 3.3, which was exposed to water vapor and was indirectly affected by the laser during the time series, showed a similar effect as in the laser-scanned area, that is, the PL intensity centered at 480 nm is doubled. This indicates that the nearby area was also affected by the laser-introduced temperature increase and halide ion migration in the humid environment. The affected area spread as far as 30 μm away from the laser-scanned area.

https://doi.org/10.1021/acsomega.4c04188
ACS Omega 2024, 9, 35744−35756

4.3. Role of E-Beam. E-beam irradiation was used to investigate the impact of exposure to a flux of energetically charged particles. Two effects of e-beam scanning were observed on the optical properties of the quasi-2D RP perovskite. One is the generation of the 525 nm PL peak, indicating the 2D to the 3D phase transition. The other is quenching of the PL of the whole flake outside of the laser-scanned area.

The e-beam irradiation is directly related to generation and growth of the 525 nm PL peak. No 525 nm peak was observed in the laser-scanned area and from locations outside the irradiated area without prior SEM imaging (section 3.3). Therefore, neither laser irradiation nor H_2O exposure generated 3D perovskite nucleation sites. After flakes were subjected to the e-beam scanning, the subsequent PL evolution trends in the laser-scanned area with water vapor (section 3.1) and without water vapor (section 3.2) were similar. Specifically, the bandgap peak at 480 nm continuously decreased in intensity whereas the peak at ∼510 nm grew in intensity while continuously redshifted toward 525 nm. The 525 nm peak reached a maximum intensity that was multiple times its initial PL intensity followed by a falling of the emission intensity. Then, both peaks diminished due to laser decomposition.

Different mechanisms have been reported for the effect of e-beam on the alteration of the physical and the optical properties of 3D perovskite including defect (halide vacancies and interstitials) formation caused by irradiation damage,[35,37,53] phase transition induced by e-beam heating,[35] and e-beam introduced ion migration.[37,54] The formation of the defect would cause quenching of the PL due to the trapping of the excitons and their nonradiative recombination. Even moderate e-beam irradiation (10 kV) could drive degradation of the MAPI perovskite and induce the quenching of the PL and CL signal.[35,37] In these reports, the PL peak was blueshifted with the shape and width of the emission spectra remaining constant. The recovery of the PL was observed after extended moderate e-beam scanning due to electron doping. Similarly, charge doping introduces an electric field that leads to ion migration. Ion migration could enhance the PL intensity in the irradiated area. However, it does not introduce a new peak.[37] The defect formation, phase transition, and ion migration are often related to crystal quality. It has been reported that for high-quality crystals, the degradation is directly in the radiation zone due to defect formation. For less uniform films, the damage can happen at the periphery of about 2−3 μm surrounding the irradiation zone due to ion migration.[53,54]

In this work, the appearance of a new PL peak is an indication of the phase transition. This is similar to the phase transition of $MAPbI_3$ under e-beam irradiation.[35] The activation of the phase transition is additionally supported by the high-intensity 525 nm peak at the high-flux e-beam irradiated areas (Figure S5). There were synergistic effects of the laser and e-beam (sections 3.1 and 3.2) in the laser scanned area. First, e-beam irradiation created the nucleation sites of the 3D perovskites. Then, the laser-introduced thermal heating accelerated the 2D to 3D phase transition. The 3D emission indicates the formation of a mixed 2D/3D phase. The growth of the 3D emission suggests a continuous phase transition to the 3D phase. For the mixed 2D/3D perovskite, the PL spectrum is reported to show the 3D-dominated emission as the electron−hole pairs originated at the lower-n phase grains are funneled to the higher-n phase grains.[18,55,56] The phase transition to the 3D perovskite supports the degradation mechanism of disproportionation into a more stable, protective, low-n surface layer and a 3D MAPI phase.[24,27,28] This degradation process is different from a mechanism proposed based on pure-phase quasi-2D $(PEA)_2(MA)_{n-1}Pb_nI_{3n+1}$ perovskite single crystal. The larger-n ($n \geq 2$) phase directly degrades into the relatively stable n = 1 phase.[29] In this case, the PL peak at a longer wavelength corresponding to the large-n phase was observed to continuously decrease, and the PL of the lower-n phase appeared at a lower wavelength and grew. This is opposite of our results. Therefore, we concluded that the quasi-2D RP perovskite with n = 3 did not degrade to a lower-n phase.

However, unlike experiments in added humidity (section 3.1), the 2D to 3D phase transition did not spread to nearby areas in the ambient environment (section 3.2). Instead, the 2D PL was quenched, and the intensity of the 3D perovskite PL peak in the nearby areas remained constant. Since there was no direct laser irradiation, water vapor exposure, and additional e-beam scanning in the nearby areas, this means that there were no additional nucleation sites generated directly due to these factors. Therefore, it is reasonable to attribute the quenching of the 480 nm PL peak at the nearby areas to the ion migration from the laser-scanned area due to a temperature gradient on the flake. The thermal activation energy of the migration of the iodide/bromine ions was experimentally determined to be about 70 kJ/mol.[57−59] These defects (e.g., ion interstitials) could trap excitons and enhance their nonradiative recombination. The quenching of the 2D PL is consistent with what has been reported for 3D perovskite after moderate e-beam exposure.[35,37] Even when the surface morphology remained the same, defects were created. Similarly, here, although quenching of the PL was observed on the whole flake, the SEM image taken after the time series shows that the surface was still smooth except for the high-fluxed areas.

Interestingly, the 2D to 3D phase transition process did not continue in the areas experienced prior high-flux e-beam scanning or spread to the other areas of the flake without direct laser illumination or moisture (section 3.2). The high concentration of defects/nucleation sites of the 3D perovskite was created during the e-beam scanning and the migration of the ion from the laser scanned area to these areas were expected as evidenced by the quenching of the 2D PL in these areas. Therefore, the ion migration alone or a small amount of ion migration is not enough to keep the phase transition going.

4.4. Synergistic Effect of Laser Exposure, Water Vapor, and E-Beam Irradiation. In the laser-scanned area, the synergistic role of water vapor is not apparent as the e-beam and laser light dominated the degradation process. The main difference in PL between experiments with water vapor and without water vapor after activation by the e-beam scanning is at the nearby areas. In the humid environment (section 3.1), the 2D-3D phase transition is not confined to the laser-scanned area. There were extended areas that exhibited the growth of the 525 nm PL peak reaching 10-folds of its original PL intensity similar to what was observed in the laser-scanned area. Other areas experienced a quenching of the PL intensity. On the other hand, for the experiments without moisture (section 3.2), the areas that exhibited the intensity of the 525 nm peak were confined to the laser-scanned area and the areas that experienced high-flux e-beam

https://doi.org/10.1021/acsomega.4c04188
ACS Omega 2024, 9, 35744−35756

scanning. In the meantime, quenching of the 2D PL was observed in almost the whole flake that was not under laser scanning. Therefore, the comparison of the PL signal in the nearby area obtained with moisture and without moisture suggests that the ion migration from the laser-scanned area to the rest of the flake happened even without moisture, which induced the 2D PL quenching. However, it was significantly enhanced in the humid environment, which accelerated the phase transition in the nearby areas.

We propose that the quenching of the 2D PL and the 2D-3D phase transition are two different stages of degradation that are related to the defect concentration and the type of the defects (i.e., ion vacancies, ion interstitials, and 3D perovskite nucleation sites). With prior low-flux e-beam scanning, low concentrations of 3D perovskite defects were generated on the flake. The continuous laser scanning created more defects (ion vacancies and ion interstitials) and promoted ion migration to the nearby area and eventually the whole flake. However, the concentration of 3D defects in the nearby area was below the threshold. Therefore, the quenching of the 2D PL peak dominated due to the trapping and recombination of the excitons at the various defect sites (ion vacancies, ion interstitials, and 3D perovskite defects). Hence, both with (section 3.1) and without water (section 3.2), extended areas that were not under continuous laser scanning exhibited 2D PL quenching.

Although the laser scanning and H_2O did not generate 3D nucleation sites, they can accelerate the phase transition process once 3D nucleation sites were generated. In the experiment with water vapor, water vapor forms the hydrates between the layered structure.[7,26,60−62] The incorporation of H_2O in the lattice could assist the ion migration, which eventually increased the 3D perovskite defect concentration to the extent that 2D to 3D perovskite transition dominates. Therefore, there are extended areas (100 μm^2) that experience the 2D to 3D phase transition even though they did not experience laser scanning (section 3.1). The moisture-enhanced ion migration was also observed in the flakes without prior e-beam irradiation (section 3.3). In this case, there were no 3D nucleation sites; therefore, the passivation of the defects dominated, which is evidenced by the enhanced 2D PL intensity in the nearby areas in section 3.3.

Note that there is heterogeneity in the as-synthesized 2D perovskite, as shown in Figure 3b. The observed inhomogeneity in PL after the time series on the whole flake is a result of a delicate balance among these synergistic factors including the laser irradiation-induced defects, the temperature gradient from laser heating, the e-beam irradiation-induced defects, the intrinsic ion migration, and the water-assisted ion migration. Therefore, it is not surprising that there was variation in the PL distribution in the experiments.

We also considered the role of the thickness of the flake in the degradation. The thickness of the majority of the flakes studied in this work is less than 1 μm, with some portion of the flakes thicker than 1 μm. Most of the excitation photons are absorbed by the halide perovskite within a few hundred nanometers. The photon infiltration exponentially decreases from the surface, which controls photoinduced ion migration in a crystal.[63,64] The ion migration induced by light could migrate both horizontally and vertically. It is reasonable to expect that ions migrate more horizontally for thinner flakes and therefore faster propagation of the degradation from the laser-scanned area to the surrounding area. However, for the thinnest flake (0.2 μm) in our experiment, shown in Figure 4, the 2D to 3D phase transition did not spread to the rest of the flake, even near the area with high-flux e-beam irradiation. In addition, in Figure 3, while the red dotted area shows a much higher PL intensity than the black dotted area, their thicknesses are comparable. This indicates that the thickness is not a main factor in the degradation involving humidity and laser irradiation. Similarly, we expect the thinner the flake, the greater the e-beam-induced damage from the scattering of the secondary electrons. This could contribute to a relatively higher ∼520 nm peak after the e-beam irradiation for the flake in Figure 2d with a thickness of 0.2 μm, while the flake in Figure 2a has a thickness of ∼0.5 μm and shows a relatively weaker 520 nm peak.

It has been reported that RP perovskites exhibit improved stability over the 3D perovskites.[24] Our results confirm the stability of the 2D RP perovskites over prolonged humidity exposure. However, the defect is critical for stability of the 2D RP perovskite. Even the low-energy, low-flux e-beam irradiation can generate the 3D nucleation sites that could compromise the stability of the 2D RP perovskite. It would not be a surprise that under electric current, the stability of the 2D RP perovskite will be compromised too. The presence of H_2O assists the propagation of the 2D to 3D phase transformation and the direct 2D degradation across the flakes.

CONCLUSIONS

In summary, the synergistic effect of three factors (laser exposure, water vapor, and e-beam irradiation) on 2D RP perovskite flakes has been investigated. The time-dependent PL of the 2D RP perovskite flakes was monitored continuously in an environmental cell for over 12 h. With prior SEM imaging, the 2D perovskite experienced the 2D to 3D phase transition process, followed by complete degradation at the laser-scanned area with or without added humidity. The 480 nm PL peak vanished, while a high-intensity 525 nm PL peak emerged with continuous laser scanning. The PL intensity then declined and eventually completely quenched due to decomposition. Without prior SEM imaging, the 2D RP perovskite did not experience a phase transition and directly decomposed. Our results indicate that e-beam irradiation initiates the phase transition by creating the 3D nucleation sites. Neither laser nor H_2O generates these nucleation sites. Laser accelerates the 2D-3D phase transition and the direct 2D decomposition process. H_2O helps the spreading of both degradation processes to the rest of the flake by enhancing the ion migration. Without added humidity, the 2D-3D phase transition was confined in a laser-scanned area.

ASSOCIATED CONTENT

Supporting Information

The Supporting Information is available free of charge at https://pubs.acs.org/doi/10.1021/acsomega.4c04188.

SEM images of the 2D RP perovskite flakes in different environmental cells; PL maps of the flake and PL spectra from additional selected points at the nearby area in the 2D RP perovskite flakes (PDF)

https://doi.org/10.1021/acsomega.4c04188
ACS Omega 2024, 9, 35744−35756

AUTHOR INFORMATION

Corresponding Author

Zhenrong Zhang − *Department of Physics, Baylor University, Waco, Texas 76798, United States;* orcid.org/0000-0003-3969-2326; Email: Zhenrong_Zhang@baylor.edu

Authors

Zhenfei Jiang − *Institute for Quantum Science and Engineering and Department of Physics and Astronomy, Texas A&M University, College Station, Texas 77843, United States;* orcid.org/0000-0002-4608-1294

Brian Ko − *Department of Physics, Baylor University, Waco, Texas 76798, United States;* orcid.org/0000-0003-3520-3484

Keith R. Berry, Jr. − *Division of Agriculture, University of Arkansas, Little Rock, Arkansas 72204, United States;* orcid.org/0000-0002-1551-7577

Xinxin Xing − *Department of Electrical & Computer Engineering and Texas Center for Superconductivity (TCSUH), University of Houston, Houston, Texas 77204, United States*

Zhenhuan Yi − *Institute for Quantum Science and Engineering and Department of Physics and Astronomy, Texas A&M University, College Station, Texas 77843, United States;* orcid.org/0000-0003-4827-1013

Alexei V. Sokolov − *Institute for Quantum Science and Engineering and Department of Physics and Astronomy, Texas A&M University, College Station, Texas 77843, United States; Department of Physics, Baylor University, Waco, Texas 76798, United States;* orcid.org/0000-0002-6879-7840

Jonathan Hu − *Department of Electrical and Computer Engineering, Baylor University, Waco, Texas 76798, United States;* orcid.org/0000-0001-6426-3051

Jiming Bao − *Department of Electrical & Computer Engineering and Texas Center for Superconductivity (TCSUH), University of Houston, Houston, Texas 77204, United States;* orcid.org/0000-0002-6819-0117

Complete contact information is available at: https://pubs.acs.org/10.1021/acsomega.4c04188

Author Contributions

[#]Z.J. and B.K. contributed equally to this study.

Notes

The authors declare no competing financial interest.

ACKNOWLEDGMENTS

Z.J. is supported by the Herman F. Heep and Minnie Belle Heep Texas A&M University Endowed Fund held/administered by the Texas A&M Foundation. K.R.B.J., Z.Z., and J.H. acknowledge the support from the Baylor OVPR Postdoctoral Fellowship Award. A.V.S. would like to thank the Robert A. Welch Foundation, grant no. A-1547. Z.Z. and B.K. acknowledge support from the National Science Foundation under grant CHE-1905043.

REFERENCES

(1) Lekesi, L. P.; Koao, L. F.; Motloung, S. V.; Motaung, T. E.; Malevu, T. Developments on Perovskite Solar Cells (PSCs): A Critical Review. *Applied Sciences* **2022**, *12* (2), 672.

(2) Wei, Y.; Cheng, Z.; Lin, J. An Overview on Enhancing the Stability of Lead Halide Perovskite Quantum Dots and Their Applications in Phosphor-Converted LEDs. *Chem. Soc. Rev.* **2019**, *48* (1), 310−350.

(3) Nandi, P.; Giri, C.; Joseph, B.; Rath, S.; Manju, U.; Topwal, D. $CH_3NH_3PbI_3$, A Potential Solar Cell Candidate: Structural and Spectroscopic Investigations. *J. Phys. Chem. A* **2016**, *120* (49), 9732−9739.

(4) Kojima, A.; Teshima, K.; Shirai, Y.; Miyasaka, T. Organometal Halide Perovskites as Visible-Light Sensitizers for Photovoltaic Cells. *J. Am. Chem. Soc.* **2009**, *131* (17), 6050−6051.

(5) Ng, C. H.; Lim, H. N.; Hayase, S.; Zainal, Z.; Huang, N. M. Photovoltaic Performances of Mono- and Mixed-Halide Structures for Perovskite Solar Cell: A Review. *Renewable and Sustainable Energy Reviews* **2018**, *90*, 248−274.

(6) Wang, R.; Mujahid, M.; Duan, Y.; Wang, Z.; Xue, J.; Yang, Y. A Review of Perovskites Solar Cell Stability. *Adv. Funct Materials* **2019**, *29* (47), 1808843.

(7) Zhang, W.; Xiong, J.; Li, J.; Daoud, W. A. Impact of Temperature-Dependent Hydration Water on Perovskite Solar Cells. *Solar RRL* **2020**, *4* (1), 1900370.

(8) Murali, B.; Dey, S.; Abdelhady, A. L.; Peng, W.; Alarousu, E.; Kirmani, A. R.; Cho, N.; Sarmah, S. P.; Parida, M. R.; Saidaminov, M. I.; Zhumekenov, A. A.; Sun, J.; Alias, M. S.; Yengel, E.; Ooi, B. S.; Amassian, A.; Bakr, O. M.; Mohammed, O. F. Surface Restructuring of Hybrid Perovskite Crystals. *ACS Energy Lett.* **2016**, *1* (6), 1119−1126.

(9) Boyd, C. C.; Cheacharoen, R.; Leijtens, T.; McGehee, M. D. Understanding Degradation Mechanisms and Improving Stability of Perovskite Photovoltaics. *Chem. Rev.* **2019**, *119* (5), 3418−3451.

(10) El-Mellouhi, F.; Marzouk, A.; Bentria, E. T.; Rashkeev, S. N.; Kais, S.; Alharbi, F. H. Hydrogen Bonding and Stability of Hybrid Organic−Inorganic Perovskites. *ChemSusChem* **2016**, *9* (18), 2648−2655.

(11) Manser, J. S.; Saidaminov, M. I.; Christians, J. A.; Bakr, O. M.; Kamat, P. V. Making and Breaking of Lead Halide Perovskites. *Acc. Chem. Res.* **2016**, *49* (2), 330−338.

(12) Wang, B.; Zhang, Z.-G.; Ye, S.; Rao, H.; Bian, Z.; Huang, C.; Li, Y. Room-Temperature Water-Vapor Annealing for High-Performance Planar Perovskite Solar Cells. *J. Mater. Chem. A* **2016**, *4* (44), 17267−17273.

(13) Ghosh, S.; Rana, D.; Pradhan, B.; Donfack, P.; Hofkens, J.; Materny, A. Vibrational Study of Lead Bromide Perovskite Materials with Variable Cations Based on Raman Spectroscopy and Density Functional Theory. *J. Raman Spectrosc.* **2021**, *52* (12), 2338−2347.

(14) Tsai, H.; Nie, W.; Blancon, J.-C.; Stoumpos, C. C.; Asadpour, R.; Harutyunyan, B.; Neukirch, A. J.; Verduzco, R.; Crochet, J. J.; Tretiak, S.; Pedesseau, L.; Even, J.; Alam, M. A.; Gupta, G.; Lou, J.; Ajayan, P. M.; Bedzyk, M. J.; Kanatzidis, M. G.; Mohite, A. D. High-Efficiency Two-Dimensional Ruddlesden−Popper Perovskite Solar Cells. *Nature* **2016**, *536* (7616), 312−316.

(15) Dong, R.; Lan, C.; Xu, X.; Liang, X.; Hu, X.; Li, D.; Zhou, Z.; Shu, L.; Yip, S.; Li, C.; Tsang, S.-W.; Ho, J. C. Novel Series of Quasi-2D Ruddlesden−Popper Perovskites Based on Short-Chained Spacer Cation for Enhanced Photodetection. *ACS Appl. Mater. Interfaces* **2018**, *10* (22), 19019−19026.

(16) Zheng, Y.; Niu, T.; Ran, X.; Qiu, J.; Li, B.; Xia, Y.; Chen, Y.; Huang, W. Unique Characteristics of 2D Ruddlesden−Popper (2DRP) Perovskite for Future Photovoltaic Application. *J. Mater. Chem. A* **2019**, *7* (23), 13860−13872.

(17) Leung, T. L.; Ahmad, I.; Syed, A. A.; Ng, A. M. C.; Popović, J.; Djurišić, A. B. Stability of 2D and Quasi-2D Perovskite Materials and Devices. *Commun. Mater.* **2022**, *3* (1), 63.

(18) Ghosh, S.; Pradhan, B.; Zhang, Y.; Roeffaers, M. B. J.; Hofkens, J.; Karki, K. J.; Materny, A. Spatial Heterogeneity of *n* -Phases Leads to Different Photophysical Properties in Quasi-Two-Dimensional Methylammonium Lead Bromide Perovskite. *J. Phys. Chem. C* **2022**, *126* (1), 478−486.

(19) Wang, M.; Shi, Z.; Fei, C.; Deng, Z. J. D.; Yang, G.; Dunfield, S. P.; Fenning, D. P.; Huang, J. Ammonium Cations with High PKa in

Perovskite Solar Cells for Improved High-Temperature Photostability. *Nat. Energy* **2023**, *8* (11), 1229−1239.
(20) Noh, M. F. M.; Arzaee, N. A.; Mumthas, I. N. N.; Mohamed, N. A.; Nasir, S. N. F. M.; Safaei, J.; Yusoff, A. R. B. M.; Nazeeruddin, M. K.; Teridi, M. A. M. High-Humidity Processed Perovskite Solar Cells. *J. Mater. Chem. A* **2020**, *8* (21), 10481−10518.
(21) Wang, R. T.; Xu, A. F.; Chen, J. Y.; Yang, L. W.; Xu, G.; Jarvis, V.; Britten, J. F. Reversing Organic−Inorganic Hybrid Perovskite Degradation in Water via PH and Hydrogen Bonds. *J. Phys. Chem. Lett.* **2019**, *10* (22), 7245−7250.
(22) Sharma, S. K.; Phadnis, C.; Das, T. K.; Kumar, A.; Kavaipatti, B.; Chowdhury, A.; Yella, A. Reversible Dimensionality Tuning of Hybrid Perovskites with Humidity: Visualization and Application to Stable Solar Cells. *Chem. Mater.* **2019**, *31* (9), 3111−3117.
(23) Schlipf, J.; Hu, Y.; Pratap, S.; Bießmann, L.; Hohn, N.; Porcar, L.; Bein, T.; Docampo, P.; Müller-Buschbaum, P. Shedding Light on the Moisture Stability of 3D/2D Hybrid Perovskite Heterojunction Thin Films. *ACS Appl. Energy Mater.* **2019**, *2* (2), 1011−1018.
(24) Wygant, B. R.; Ye, A. Z.; Dolocan, A.; Vu, Q.; Abbot, D. M.; Mullins, C. B. Probing the Degradation Chemistry and Enhanced Stability of 2D Organolead Halide Perovskites. *J. Am. Chem. Soc.* **2019**, *141* (45), 18170−18181.
(25) Segovia, R.; Qu, G.; Peng, M.; Sun, X.; Shi, H.; Gao, B. Evolution of Photoluminescence, Raman, and Structure of CH3NH3PbI3 Perovskite Microwires Under Humidity Exposure. *Nanoscale Res. Lett.* **2018**, *13* (1), 79.
(26) Schlipf, J.; Bießmann, L.; Oesinghaus, L.; Berger, E.; Metwalli, E.; Lercher, J. A.; Porcar, L.; Müller-Buschbaum, P. In Situ Monitoring the Uptake of Moisture into Hybrid Perovskite Thin Films. *J. Phys. Chem. Lett.* **2018**, *9* (8), 2015−2021.
(27) Koh, T. M.; Shanmugam, V.; Guo, X.; Lim, S. S.; Filonik, O.; Herzig, E. M.; Müller-Buschbaum, P.; Swamy, V.; Chien, S. T.; Mhaisalkar, S. G.; Mathews, N. Enhancing Moisture Tolerance in Efficient Hybrid 3D/2D Perovskite Photovoltaics. *J. Mater. Chem. A* **2018**, *6* (5), 2122−2128.
(28) Wygant, B. R.; Geberth, G. T.; Ye, A. Z.; Dolocan, A.; Cotton, D. E.; Roberts, S. T.; Vanden Bout, D. A.; Mullins, C. B. Moisture-Driven Formation and Growth of Quasi-2-D Organolead Halide Perovskite Crystallites. *ACS Appl. Energy Mater.* **2020**, *3* (7), 6280−6290.
(29) Tang, J.; Tian, W.; Zhao, C.; Sun, Q.; Zhang, C.; Cheng, H.; Shi, Y.; Jin, S. Imaging the Moisture-Induced Degradation Process of 2D Organolead Halide Perovskites. *ACS Omega* **2022**, *7* (12), 10365−10371.
(30) deQuilettes, D. W.; Zhang, W.; Burlakov, V. M.; Graham, D. J.; Leijtens, T.; Osherov, A.; Bulović, V.; Snaith, H. J.; Ginger, D. S.; Stranks, S. D. Photo-Induced Halide Redistribution in Organic−Inorganic Perovskite Films. *Nat. Commun.* **2016**, *7* (1), 11683.
(31) Vicente, J. R.; Kordesch, M. E.; Chen, J. Stabilization of Mixed-Halide Lead Perovskites under Light by Photothermal Effects. *Journal of Energy Chemistry* **2021**, *63*, 8−11.
(32) Tian, Y.; Peter, M.; Unger, E.; Abdellah, M.; Zheng, K.; Pullerits, T.; Yartsev, A.; Sundström, V.; Scheblykin, I. G. Mechanistic Insights into Perovskite Photoluminescence Enhancement: Light Curing with Oxygen Can Boost Yield Thousandfold. *Phys. Chem. Chem. Phys.* **2015**, *17* (38), 24978−24987.
(33) Fang, H.; Yang, J.; Tao, S.; Adjokatse, S.; Kamminga, M. E.; Ye, J.; Blake, G. R.; Even, J.; Loi, M. A. Unravelling Light-Induced Degradation of Layered Perovskite Crystals and Design of Efficient Encapsulation for Improved Photostability. *Adv. Funct Materials* **2018**, *28* (21), 1800305.
(34) Fiorentino, F.; Albaqami, M. D.; Poli, I.; Petrozza, A. Thermal- and Light-Induced Evolution of the 2D/3D Interface in Lead-Halide Perovskite Films. *ACS Appl. Mater. Interfaces* **2022**, *14* (30), 34180−34188.
(35) Xiao, C.; Li, Z.; Guthrey, H.; Moseley, J.; Yang, Y.; Wozny, S.; Moutinho, H.; To, B.; Berry, J. J.; Gorman, B.; Yan, Y.; Zhu, K.; Al-Jassim, M. Mechanisms of Electron-Beam-Induced Damage in Perovskite Thin Films Revealed by Cathodoluminescence Spectroscopy. *J. Phys. Chem. C* **2015**, *119* (48), 26904−26911.
(36) Dang, Z.; Luo, Y.; Xu, Y.; Gao, P.; Wang, X.-S. Transformation and Degradation of Metal Halide Perovskites Induced by Energetic Electrons and Their Practical Implications. *Nano Futures* **2021**, *5* (3), No. 032001.
(37) Yuan, H.; Debroye, E.; Janssen, K.; Naiki, H.; Steuwe, C.; Lu, G.; Moris, M.; Orgiu, E.; Uji-i, H.; De Schryver, F.; Samorì, P.; Hofkens, J.; Roeffaers, M. Degradation of Methylammonium Lead Iodide Perovskite Structures through Light and Electron Beam Driven Ion Migration. *J. Phys. Chem. Lett.* **2016**, *7* (3), 561−566.
(38) Chen, S.; Zhang, X.; Zhao, J.; Zhang, Y.; Kong, G.; Li, Q.; Li, N.; Yu, Y.; Xu, N.; Zhang, J.; Liu, K.; Zhao, Q.; Cao, J.; Feng, J.; Li, X.; Qi, J.; Yu, D.; Li, J.; Gao, P. Atomic Scale Insights into Structure Instability and Decomposition Pathway of Methylammonium Lead Iodide Perovskite. *Nat. Commun.* **2018**, *9* (1), 4807.
(39) Qin, Z.; Dai, S.; Gajjela, C. C.; Wang, C.; Hadjiev, V. G.; Yang, G.; Li, J.; Zhong, X.; Tang, Z.; Yao, Y.; Guloy, A. M.; Reddy, R.; Mayerich, D.; Deng, L.; Yu, Q.; Feng, G.; Calderon, H. A.; Robles Hernandez, F. C.; Wang, Z. M.; Bao, J. Spontaneous Formation of 2D/3D Heterostructures on the Edges of 2D Ruddlesden−Popper Hybrid Perovskite Crystals. *Chem. Mater.* **2020**, *32* (12), 5009−5015.
(40) Ko, B. A.; Berry, K.; Qin, Z.; Sokolov, A. V.; Hu, J.; Scully, M. O.; Bao, J.; Zhang, Z. Resonant Degenerate Four-Wave Mixing at the Defect Energy Levels of 2D Organic−Inorganic Hybrid Perovskite Crystals. *ACS Appl. Mater. Interfaces* **2021**, *13* (48), 57075−57083.
(41) Cho, H.; Jeong, S.-H.; Park, M.-H.; Kim, Y.-H.; Wolf, C.; Lee, C.-L.; Heo, J. H.; Sadhanala, A.; Myoung, N.; Yoo, S.; Im, S. H.; Friend, R. H.; Lee, T.-W. Overcoming the Electroluminescence Efficiency Limitations of Perovskite Light-Emitting Diodes. *Science* **2015**, *350* (6265), 1222−1225.
(42) Wei, H.; Fang, Y.; Mulligan, P.; Chuirazzi, W.; Fang, H.-H.; Wang, C.; Ecker, B. R.; Gao, Y.; Loi, M. A.; Cao, L.; Huang, J. Sensitive X-Ray Detectors Made of Methylammonium Lead Tribromide Perovskite Single Crystals. *Nature Photon* **2016**, *10* (5), 333−339.
(43) Tyagi, P.; Arveson, S. M.; Tisdale, W. A. Colloidal Organohalide Perovskite Nanoplatelets Exhibiting Quantum Confinement. *J. Phys. Chem. Lett.* **2015**, *6* (10), 1911−1916.
(44) Yang, Y.; Yan, Y.; Yang, M.; Choi, S.; Zhu, K.; Luther, J. M.; Beard, M. C. Low Surface Recombination Velocity in Solution-Grown CH3NH3PbBr3 Perovskite Single Crystal. *Nat. Commun.* **2015**, *6* (1), 7961.
(45) Wang, K.; Wu, C.; Jiang, Y.; Yang, D.; Wang, K.; Priya, S. Distinct Conducting Layer Edge States in Two-Dimensional (2D) Halide Perovskite. *Sci. Adv.* **2019**, *5* (7), No. eaau3241.
(46) Li, H.; Wu, J.; Huang, X.; Lu, G.; Yang, J.; Lu, X.; Xiong, Q.; Zhang, H. Rapid and Reliable Thickness Identification of Two-Dimensional Nanosheets Using Optical Microscopy. *ACS Nano* **2013**, *7* (11), 10344−10353.
(47) Okamoto, T.; Shahjahan, Md.; Biju, V. Shape-Dependent Kinetics of Halide Vacancy Filling in Organolead Halide Perovskites. *Advanced Optical Materials* **2021**, *9* (19), 2100355.
(48) He, J.; Fang, W.-H.; Long, R.; Prezhdo, O. V. Superoxide/Peroxide Chemistry Extends Charge Carriers' Lifetime but Undermines Chemical Stability of $CH_3NH_3PbI_3$ Exposed to Oxygen: Time-Domain *Ab Initio* Analysis. *J. Am. Chem. Soc.* **2019**, *141* (14), 5798−5807.
(49) He, J.; Fang, W.-H.; Long, R.; Prezhdo, O. V. Why Oxygen Increases Carrier Lifetimes but Accelerates Degradation of $CH_3NH_3PbI_3$ under Light Irradiation: Time-Domain Ab Initio Analysis. *J. Am. Chem. Soc.* **2020**, *142* (34), 14664−14673.
(50) Aristidou, N.; Eames, C.; Sanchez-Molina, I.; Bu, X.; Kosco, J.; Islam, M. S.; Haque, S. A. Fast Oxygen Diffusion and Iodide Defects Mediate Oxygen-Induced Degradation of Perovskite Solar Cells. *Nat. Commun.* **2017**, *8* (1), 15218.
(51) Chouhan, L.; Ghimire, S.; Biju, V. Blinking Beats Bleaching: The Control of Superoxide Generation by Photo-ionized Perovskite Nanocrystals. *Angew. Chem. Int. Ed* **2019**, *58* (15), 4875−4879.

https://doi.org/10.1021/acsomega.4c04188
ACS Omega 2024, 9, 35744−35756

(52) Eperon, G. E.; Habisreutinger, S. N.; Leijtens, T.; Bruijnaers, B. J.; van Franeker, J. J.; deQuilettes, D. W.; Pathak, S.; Sutton, R. J.; Grancini, G.; Ginger, D. S.; Janssen, R. A. J.; Petrozza, A.; Snaith, H. J. The Importance of Moisture in Hybrid Lead Halide Perovskite Thin Film Fabrication. *ACS Nano* **2015**, *9* (9), 9380−9393.
(53) Chen, X.; Wang, Z. Investigating Chemical and Structural Instabilities of Lead Halide Perovskite Induced by Electron Beam Irradiation. *Micron* **2019**, *116*, 73−79.
(54) Yan, S.; Shen, Z.; Liu, Z.; Liu, M.; Ma, N.; Cheng, Y.; Gao, Y.; Ahmed, S.; Lu, Z.-H.; Luo, J.; Li, L.; Tang, J. Study of Electron Beam-Initiated Structure Damage and Recovery of Perovskite Thin Films. *J. Phys. Chem. C* **2024**, *128* (15), 6455−6463.
(55) Qin, C.; Matsushima, T.; Potscavage, W. J.; Sandanayaka, A. S. D.; Leyden, M. R.; Bencheikh, F.; Goushi, K.; Mathevet, F.; Heinrich, B.; Yumoto, G.; Kanemitsu, Y.; Adachi, C. Triplet Management for Efficient Perovskite Light-Emitting Diodes. *Nat. Photonics* **2020**, *14* (2), 70−75.
(56) Yuan, M.; Quan, L. N.; Comin, R.; Walters, G.; Sabatini, R.; Voznyy, O.; Hoogland, S.; Zhao, Y.; Beauregard, E. M.; Kanjanaboos, P.; Lu, Z.; Kim, D. H.; Sargent, E. H. Perovskite Energy Funnels for Efficient Light-Emitting Diodes. *Nat. Nanotechnol.* **2016**, *11* (10), 872−877.
(57) Azpiroz, J. M.; Mosconi, E.; Bisquert, J.; De Angelis, F. Defect Migration in Methylammonium Lead Iodide and Its Role in Perovskite Solar Cell Operation. *Energy Environ. Sci.* **2015**, *8* (7), 2118−2127.
(58) Eames, C.; Frost, J. M.; Barnes, P. R. F.; O'Regan, B. C.; Walsh, A.; Islam, M. S. Ionic Transport in Hybrid Lead Iodide Perovskite Solar Cells. *Nat. Commun.* **2015**, *6* (1), 7497.
(59) Hoke, E. T.; Slotcavage, D. J.; Dohner, E. R.; Bowring, A. R.; Karunadasa, H. I.; McGehee, M. D. Reversible Photo-Induced Trap Formation in Mixed-Halide Hybrid Perovskites for Photovoltaics. *Chem. Sci.* **2015**, *6* (1), 613−617.
(60) Huang, H.; Pradhan, B.; Hofkens, J.; Roeffaers, M. B. J.; Steele, J. A. Solar-Driven Metal Halide Perovskite Photocatalysis: Design, Stability, and Performance. *ACS Energy Lett.* **2020**, *5* (4), 1107−1123.
(61) Koushik, D.; Hazendonk, L.; Zardetto, V.; Vandalon, V.; Verheijen, M. A.; Kessels, W. M. M.; Creatore, M. Chemical Analysis of the Interface between Hybrid Organic−Inorganic Perovskite and Atomic Layer Deposited Al_2O_3. *ACS Appl. Mater. Interfaces* **2019**, *11* (5), 5526−5535.
(62) Kodenkandath, T. A.; Wiley, J. B. Synthesis and Structure of a Double-Layered Perovskite and Its Hydrate, K2SrTa2O7·mH2O (m = 0, 2). *Mater. Res. Bull.* **2000**, *35* (10), 1737−1742.
(63) Ceratti, D. R.; Rakita, Y.; Cremonesi, L.; Tenne, R.; Kalchenko, V.; Elbaum, M.; Oron, D.; Potenza, M. A. C.; Hodes, G.; Cahen, D. Self-Healing Inside $APbBr_3$ Halide Perovskite Crystals. *Adv. Mater.* **2018**, *30* (10), 1706273.
(64) Choi, H.; Ke, J. C.-R.; Skalsky, S.; Castle, C. A.; Li, K.; Moore, K. L.; Flavell, W. R.; Parkinson, P. Visualizing the Role of Photoinduced Ion Migration on Photoluminescence in Halide Perovskite Grains. *J. Mater. Chem. C* **2020**, *8* (22), 7509−7518.

https://doi.org/10.1021/acsomega.4c04188
ACS Omega 2024, 9, 35744−35756